



Tuning of defects induced visible photoluminescence by swift heavy ion irradiation and thermal annealing in zinc oxide films

R.G. Singh^{a, **}, Himanshi Gupta^b, R.M. Mehra^c, Fouran Singh^{b,*}

^a Department of Physics, Bhagini Nivedita College University of Delhi, New Delhi -110043, India

^b Materials Science Group, Inter University Accelerator Centre, Aruna Asaf Ali Marg, New Delhi-110067, India

^c School of Electronics and Communication Engineering, Sharda University, Greater Noida, U.P., 201308, India

ARTICLE INFO

Keywords:

ZnO
Photoluminescence
Oxygen vacancies
Vacancies clusters
Swift heavy ions

ABSTRACT

Present study reports the influence of electronic energy deposition on sol-gel grown zinc oxide thin films with different type of microstructures for tailoring the defects induced photoluminescence properties. The microstructure of the films was modified by the controlled thermal annealing and the nature of defects were tuned by **swift heavy ions (SHI)** irradiations at varying ion fluences of such thin films. It is observed that all the films show two emission bands in the spectral range of 350 nm–1000 nm; (i) a very weak UV-emission band and (ii) a broad visible emission band. The UV-emission band is attributed to the band to band transition while the visible emission to the deep-level defects. The maximum visible emission lies in the green emission region which enhanced with increasing annealing temperature for the samples annealed in controlled Argon gas environment in comparison of samples annealed in an oxygen environment. The intensity of the visible emission band was found to be increased with ion irradiation at low ion fluences while showing reduction at higher ion fluences along with peak broadening. The films annealed at higher annealing temperature exhibit shifting of peak maximum from green region to red region at higher fluences. The peak shifting and peak broadening at higher ion fluences could be attributed to the formation of the high density of complex defects such vacancies cluster and ionized oxygen vacancies in the lattice as tuned under the influence of electronic energy deposition through SHI irradiations. Thus, it is suggested that the intense luminescence induced by the defects could be tuned in controlled manner by selecting the proper irradiations parameters and thus it would be very interesting for the development of the optoelectronic applications.

1. Introduction

Zinc oxide is an n-type semiconductor exhibiting wurtzite hexagonal structure at ambient conditions. It has a wide bandgap of 3.37 eV and high excitonic binding energy of 60 meV (greater than room temperature thermal energy of around 25 meV) (Özgür et al., 2005a). ZnO unique properties make it a suitable candidate for many applications such as solar cell (Hüpkes et al., 2012; Bhosle et al., 2007), light-emitting diode (LED) (Xu et al., 2006; Willander et al., 2009; Ryu et al., 2006), gas sensors (Zhu and Zeng, 2017; Shishyanu et al., 2005), UV detectors (Vettumperumal et al., 2014; Soni et al., 2020), etc. Investigation on the luminescence properties of ZnO is still going on to fully utilize its properties for solid-state light-emitting applications. Generally, ZnO shows a sharp emission band in the ultra-violet region (UV) and a broad

emission band in the visible region of solar spectrum (Özgür et al., 2005b). The emission band in UV-region known as near band edge emission has been reported widely and attributed to exciton recombination or the band to band transition (conduction band to valence band or vice-versa). While the emission band in the visible region known as deep-level emission attributed to the extrinsic and intrinsic defects present in the ZnO films. The intrinsic defects (sometimes called as native point defects) in ZnO are zinc vacancy (V_{Zn}), zinc interstitial (Zn_i), oxygen vacancy (V_O), oxygen interstitial (O_i), zinc and oxygen antisites (O_{Zn} and Zn_O) and so on (Oba et al., 2011; Look et al., 2005). In which Zn_i acts as a shallow donor, V_{Zn} acts as a shallow acceptor, V_O act as a deep donor, and O_i act as a deep acceptor (Lyons et al., 2017; Janotti and Van de Walle, 2007). In particular, in the case of ZnO, it is difficult to avoid intrinsic defects completely due to its non-stoichiometric

* Corresponding author.

** Corresponding author.

E-mail addresses: rgsnsc@gmail.com (R.G. Singh), fouran@gmail.com (F. Singh).

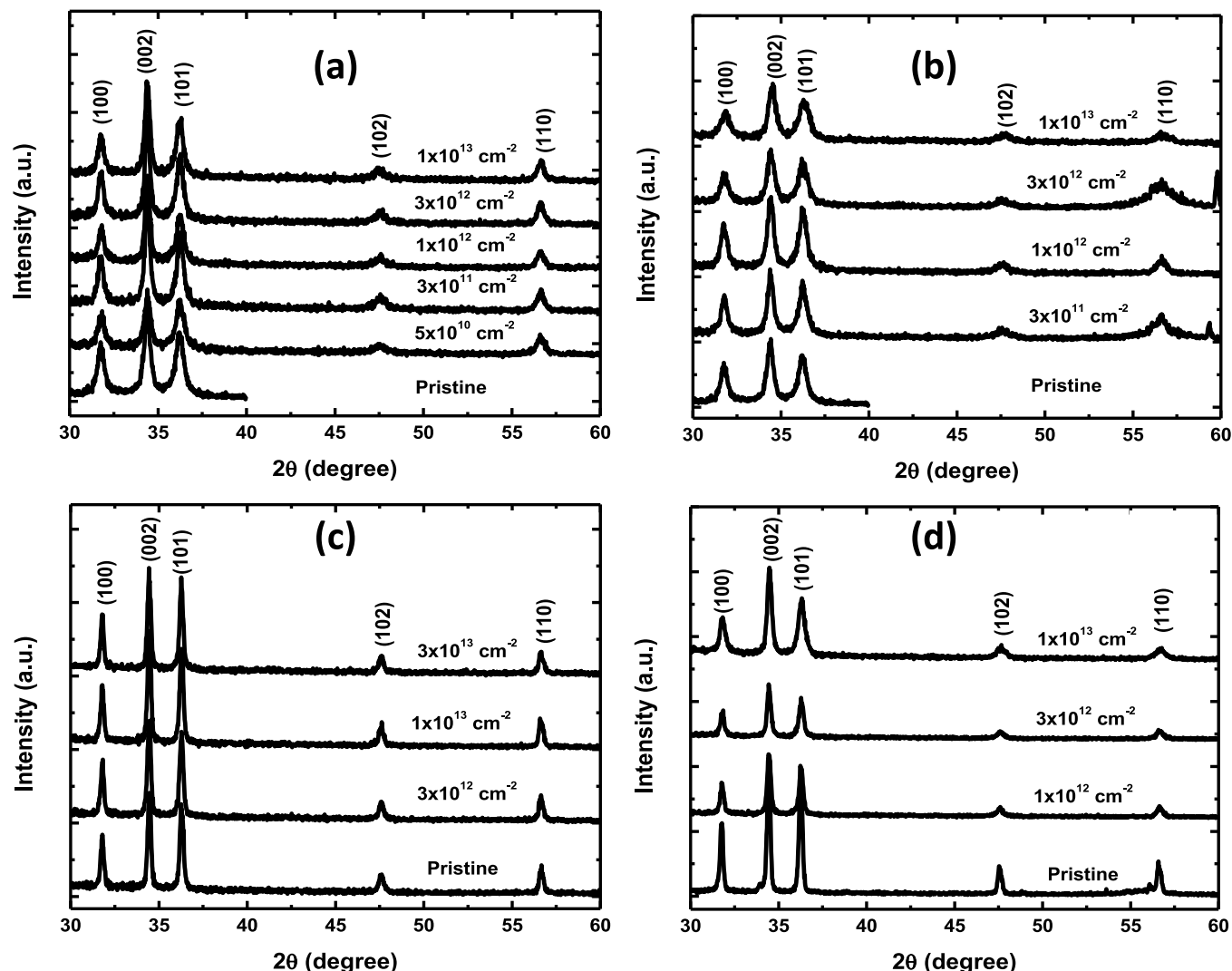


Fig.-1. XRD pattern of; (a) 500 °C–Ar annealed films irradiated with 50 MeV–Ni ions (Set-A), (b) 500 °C–Ar annealed films irradiated with 120 MeV–Au ions (Set-B), (c) 700 °C–Ar annealed films irradiated with 50 MeV–Ni ions (Set-C), and (d) 700 °C–Ar annealed films irradiated with 120 MeV–Au ions (Set-D).

behavior. Nevertheless, the luminescence behavior of ZnO can be tuned in a controlled manner by controlling the number of defects according to the desire application. Luminescence properties of ZnO get affected by various parameters such as a method of deposition (Thongpool et al., 2019; Fan et al., 2005; Barbagiovanni et al., 2015), the structure of ZnO (Cao et al., 2019; Kabir et al., 2018; Vanheusden et al., 1996), type of dopant (Musavi et al., 2019; Naik et al., 2020; Khranovskyy et al., 2017), doping concentration (Gupta et al., 2019; Kim et al., 2012; Horng et al., 2016), annealing temperature (Ambrosio et al., 2019; Kang et al., 2004) and environment (Gruzintsev and Yakimov, 2005; Singh et al., 2011a) also plays a crucial role in luminescence properties of ZnO.

It has been reported previously by our group (Singh et al., 2011a), that annealing environment or annealing temperature has a significant effect on the luminescence properties of ZnO thin films. We showed that the efficiency of visible luminescence increases with increasing annealing temperature and also in the reduced environment (annealing in Ar-gas) the intensity of visible emission evolved which was attributed to increase in the concentration of deep-level defects. In another report by H. Kang et al. (2004), also supports our previous work that the intensity of visible emission increases with an increase in annealing temperature. But the origin behind visible luminescence is contradictory in many reports and the research is still going on to find out the exact origin

of visible emission such as green emission. Further, it is well known that visible luminescence in ZnO can be tuned by controlling the type and concentration of defects present in the system. In this context, ion irradiation is the best tool to create defects into a material in a controlled manner by varying irradiation parameters such as ion species, ion beam current, ion fluences, and ion energy, etc. There are some reports available on the effect of ion irradiation on luminescence properties (Kumar et al., 2013a; Gautam et al., 2015; Singh et al., 2009; Sharma et al., 2011). Recently, H. Gupta et al. (2019), reported that with ion irradiation the visible emission can be tuned. Thus it would be interesting to study the luminescence behavior of ZnO thin films by combining annealing conditions and ion irradiation.

In view of this, the sol-gel spin coating grown films annealed at 500 °C in an oxygen environment, 500 °C in an argon environment, and 700 °C in argon environment are irradiated using 50 MeV Ni and 120 MeV Au ions with different fluences. Two annealing temperatures were chosen to have two different types of microstructure and surface morphology. The nanostructured films are modified by SHIs with varying electronic energy deposition into the ZnO films. These ions loose negligible energy in nuclear scattering as compared to the electronic energy deposition and the range of the ions is much larger than the thickness of the ZnO films. Therefore, ions are implanted deep inside the

Si substrates and the modification in the ZnO thin films are mainly expected due the electronic energy deposition via these incident ions in the ZnO films.

2. Experimental details

ZnO thin films of thickness about 300 nm (Gupta et al., 2020) were deposited on a silicon substrate via the sol-gel spin coating method. The details of film preparation were reported elsewhere (Singh et al., 2011a). The as-deposited films were thermally annealed in two different environments (oxygen and argon) at two different annealing temperatures (500 °C and 700 °C) for 1 h. Further, all the thin films were irradiated with 50 MeV Ni and 120 MeV Au ions at varying ion fluences using 15 UD tandem accelerator at IUAC, New Delhi, India. For irradiation, all the samples were mounted on a four-face copper block of a ladder after that ladder was mounted in a high vacuum irradiation chamber. The beam size and current fixed at $1 \times 1 \text{ cm}^2$ and 1 pA, respectively for both the ion beams. All films were irradiated for ion fluence of 5×10^{10} ions/cm (Hüpkes et al., 2012), 3×10^{11} ions/cm (Hüpkes et al., 2012), 1×10^{12} ions/cm (Hüpkes et al., 2012), 3×10^{12} ions/cm (Hüpkes et al., 2012), and 1×10^{13} ions/cm (Hüpkes et al., 2012). Before and after irradiation ZnO films were characterized by GAXRD, AFM, and photoluminescence spectroscopy (PL) techniques. GAXRD was carried out using Bruker-D8 advanced diffractometer to study the structural modifications of the irradiated films. AFM images were taken using Digital Nanoscope III-a SPM to study the surface topography of films. To study the effect of ion irradiation on luminescence properties of ZnO PL-measurements were carried out using Michelle 900 spectrograph under 325 nm excitation of He-Cd laser.

Further, the nuclear (S_n) for 50 MeV Ni ions and 120 MeV Au ions were found to be 0.04937 keV/nm and 0.445 keV/nm, respectively while the electronic energy loss (S_e) 50 MeV Ni ions and 120 MeV Au ions were found to be 12.67 keV/nm and 24.67 keV/nm, respectively and were estimated using SRIM-2013. It has been reported that the threshold value for electronic energy loss (S_{eth}) is around 10.18 keV/nm (Gupta et al., 2019) for ZnO. As the electronic energy loss for both the ions is greater than nuclear energy loss thus the modification in material properties would occur due to electronic energy loss.

For this study we divided our samples into five-set of samples, (i) the first set of samples (named as Set-A) consist ZnO thin films annealed in Argon environment at 500 °C and irradiated with 50 MeV-Ni ions, and (ii) the second set of samples (named as Set-B) consist ZnO thin films annealed in Argon environment at 500 °C and irradiated with 120 MeV-Au ions, (iii) the third set of samples (named as Set-C) consist ZnO thin films annealed in Argon environment at 700 °C and irradiated with 50 MeV-Ni ions, and (iv) the fourth set of samples (named as Set-D) consist ZnO thin films annealed in Argon environment at 700 °C and irradiated with 120 MeV-Au ions, and (v) the fifth set of samples (named as Set-E) consist ZnO thin films annealed in an oxygen environment at 500 °C and irradiated with 50 MeV-Ni ions.

3. Results and discussions

3.1. Structural properties

Fig.-1(a), (a'), (b), and (b') show the GAXRD pattern of Set-A, Set-B, Set-C, and Set-D films, respectively with different ion fluences. The XRD pattern for the samples of all four sets shows (100), (002), (101), (102), and (110) diffraction peaks. This indicates hexagonal wurtzite structure [JCPDS 36–1451] of all of the films and all films possess polycrystalline nature. The most preferred orientation of all of the films is along the c-axis. The width of (002) diffraction peak increases with the increase of ion fluence for Au ions, while almost remains the same for the films irradiated using Ni ions as can be seen from the XRD pattern of Set-A, Set-B, Set-C, and Set-D films. The average grain size and lattice parameters ('a' & 'c') of the films of all four sets were estimated using the

Table-1

Estimated values of average grain size (nm) and lattice parameters 'a' (Å) and 'c' (Å) of 50 MeV-Ni and 120 MeV-Au irradiated films with annealing temperature of 500 °C and 700 °C.

Ion energy & species	Annealing Temp. (°C)	Fluence (ions/cm ²)	Av. Grain Size (nm)	c (Å)	a (Å)
50 MeV-Ni	500	Pristine	31.2	5.2089	3.2488
		3×10^{11}	30.1	5.2066	3.2491
		1×10^{12}	31.8	5.2069	3.2472
		3×10^{12}	30.7	5.2066	3.2485
		1×10^{13}	28.3	5.2082	3.2481
	700	Pristine	47.8	5.2017	3.2481
		3×10^{12}	45.2	5.2034	3.2476
		1×10^{13}	46.9	5.2034	3.2476
		3×10^{13}	45	5.2038	3.2484
		Pristine	21.2	5.2089	3.2488
120 MeV-Au	500	3×10^{11}	23.5	5.2063	3.2478
		1×10^{12}	22.5	5.2055	3.2491
		3×10^{12}	19.1	5.2035	3.2464
		1×10^{13}	19.1	5.1928	3.2439
		Pristine	45	5.2044	3.251
	700	1×10^{12}	35	5.2023	3.2484
		3×10^{12}	30	5.2022	3.247
		1×10^{13}	28	5.1983	3.2454

standard formula for hexagonal structure (Singh et al., 2011a). The values of these parameters are tabulated in Table- 1. From this table, it can be seen that Ni irradiated films (Set-A and Set-C) show less impact on structural properties, as compared to Au irradiated films (Set-C), which shows a decrease in lattice parameter 'c' with an increase in ion fluences. This indicates that the irradiation with Au ions induces compressive stress along the c-axis.

For a better understanding of the effect of SHI irradiation on the lattice parameters; the values of lattice parameter 'c' for Set-A and Set-B samples are plotted as a function of ion fluences as shown in Fig.-2(a). This figure reveals that Au ions induce the stresses on the lattice, while the Ni ions were not able to induce any stresses. The stress effects pronounced for the multiple ions impact and keep increases with the increase of ion fluences. The presence of intrinsic stress is attributed to the accumulation of crystallographic flaws such as the growth of crystallites at equilibrium sites and non-stoichiometry which were built in the film during SHI irradiation. The residual stress along the c-axis tends to lower the length of the c-axis. During the irradiation treatment, these crystallites gain a different types of imperfection in the structure. At moderate ion fluence, crystallites deplete to relatively equilibrium sites in the crystal lattice with lower surface energy. It has been observed that these parameters drastically change due to the high value of S_e . It would be better to note that as the fluence of Ni ion irradiation is 30 times more as compared to Au ions. An thus, the strong induction of strain by Au ions could be attributed to the high density of electronic excitations. The high S_e is responsible for the lattice imperfection and broadening in the XRD peak which is in well agreement with the literature (Kumar et al., 2013b; Singh et al., 2011b).

The structural, electrical, and optical properties of the ZnO films can be correlated with microstructural characteristics. The origin of lattice strain can be attributed to the excess volume of grain boundaries associated with vacancies and vacancy clusters as reported by Singh et al. (2011b). The mean magnitude of the local lattice strains in nanocrystalline samples could be estimated from the XRD pattern. The strain in Au irradiated films annealed in Ar-environment at 500 °C is estimated by a uniform deformation model (UDM) which is the modified form of Williamson-Hall (W-H) method (Thandavan et al., 2015). According to the modified W-H method the strain (ϵ) and particle size (D) can be related as follows (Thandavan et al., 2015);

$$\beta_{hkl} \cos\theta = \frac{K\lambda}{D} + 4\epsilon \sin\theta$$

Where λ is the wavelength of X-rays used for recording the XRD pattern,

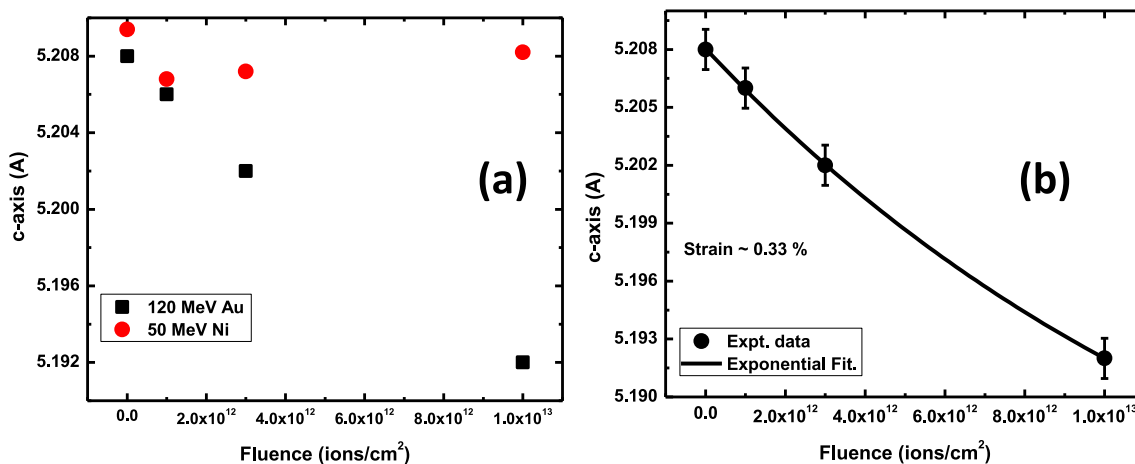


Fig. 2. (a) Variation in strain along c-axis with ion fluences for 50 MeV–Ni and 120 MeV–Au ion irradiated films annealed at 500 °C–Ar, (b) Variation in strain along c-axis with ions fluences for 120 MeV–Au ion irradiated films annealed at 500 °C–Ar.

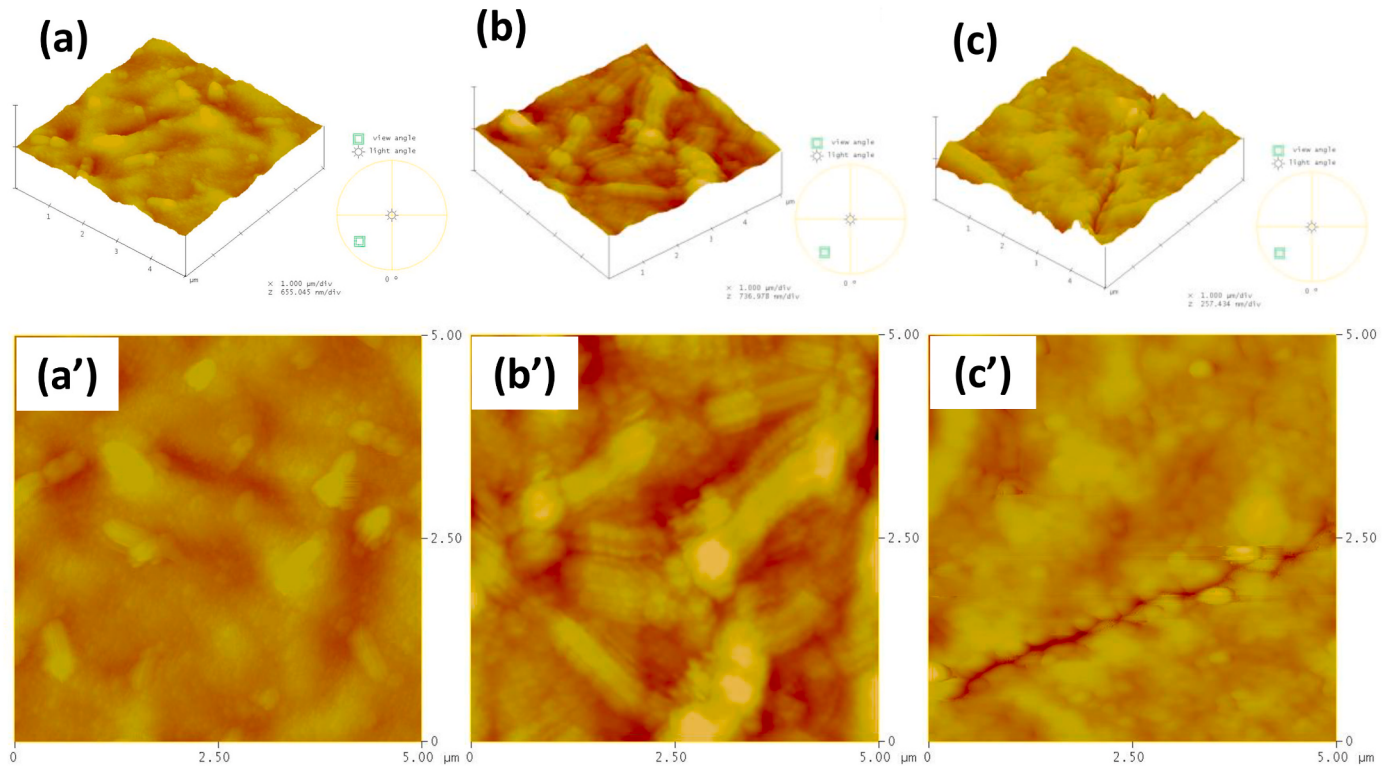


Fig. 3. 3-D AFM images of 500 °C–Ar annealed (a) pristine, (b) 50 MeV–Ni irradiated ZnO film, (c) 120 MeV–Au irradiated ZnO film, and 2-D AFM images of 500 °C–Ar annealed (a') pristine, (b') 50 MeV–Ni irradiated ZnO film, (c') 120 MeV–Au irradiated ZnO film.

K is the shape factor (0.9) and θ is the Bragg's angle of diffraction. The W-H method provides an apparent size parameter of coherently scattering domains (y-intercept) and the values of the mean square strain (slope of the graph). Fig.-2(b) shows the experimental data of Set-D samples fitted with the W-H method and from the fitting, the percentage of induced strain into ZnO through Au ion irradiation comes around 0.33%. Thus from the XRD pattern, it is clear that the ion irradiation with Au ions having Se value approximately two times greater than Ni ions have more impact on structural properties of ZnO thin films despite variation in annealing temperature. It is noteworthy that such energetic ions implanted deep into the Si substrate and induced localized thermal spikes in a cylinder of radius 5–10 nm, which can lead to stress due to the

mismatch between the thermal expansion of the Si substrates and the ZnO films. However, the induced stress in the Si substrate is insignificant to cause any appreciable modifications in such polycrystalline ZnO films (Kumar et al., 2013b; Singh et al., 2011b).

3.2. Surface morphology

The surface topography of the pristine and irradiated films is studied using AFM in the tapping mode. Fig.-3 shows the three and two-dimensional micrograph in 1 × 1 μm² of the pristine sample, 50-MeV Ni irradiated, and 120-MeV Au irradiated film for a fixed ion fluence of 1 × 10¹³ ions/cm² and all films were annealed in Ar-gas at 500 °C. On

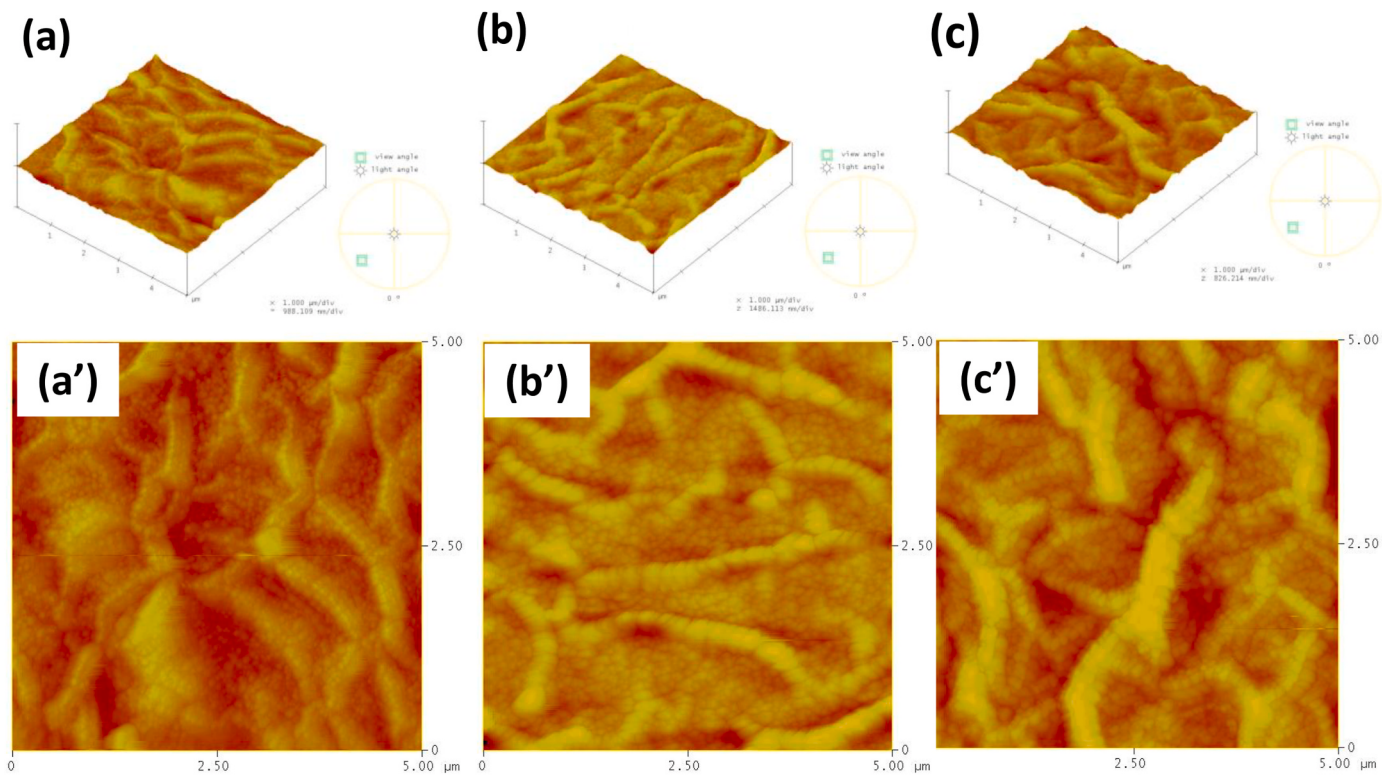


Fig. 4. 3-D AFM images of 700 °C–Ar annealed (a) pristine, (b) 50 MeV–Ni irradiated ZnO film, (c) 120 MeV–Au irradiated ZnO film, and 2-D AFM images of 700 °C–Ar annealed (a') pristine, (b') 50 MeV–Ni irradiated ZnO film, (c') 120 MeV–Au irradiated ZnO film.

the other hand, Fig. 4 shows the three and two-dimensional micrograph in $1 \times 1 \mu\text{m}^2$ of the pristine sample, 50-MeV Ni irradiated, and 120-MeV Au irradiated film for a fixed ion fluence of 1×10^{13} ions/cm 2 and all films were annealed in Ar-gas at 700 °C. From the AFM images of these films, it can be seen that higher annealing temperature and ion fluence leads to homogeneous and uniform film. Such a change in the size and shape of the crystallites is attributed to the high density of electronic excitations induced by SHI irradiation under multiple ion impacts in the near-surface region.

3.3. Photoluminescence properties

Fig. 5(a), (b), (c), and (d) shows the PL spectra of samples of Set-A, samples of Set-B, samples of Set-C, and samples of Set-D, respectively. As can be seen from PL-spectra of all the pristine samples from all four sets exhibit a very weak UV emission band peaking around 400 nm and a broad visible emission band covering the whole visible region from 410 nm to 800 nm. The UV emission band corresponds to the near band edge emission that transition from the conduction band to the valence band. While the visible emission band attributed to the deep level defects present in the material. The visible band is peaking around 530 nm which means that the green emission is pronounced in all of the pristine samples irrespective of annealing temperature as can be seen from PL spectra. The origin of green emission will be discussed later in the manuscript. Further, PL-spectra of the films annealed at 500 °C (Set-A and Set-B) exhibit different behavior than films annealed at 700 °C (Set-C and Set-D) after ion irradiation with energetic Ni and Au ions. However, it is observed that the SHI irradiation for both Au and Ni ions show a similar effect on the PL spectra that is the effect of ions is similar for the samples annealed at the same temperature. Firstly, we will discuss about the PL-spectra of the irradiated films annealed at 500 °C and is shown in Fig. 5(a) and (b). From the PL-spectra of Set-A and Set-B films, it can be seen that the intensity of green emission increases with increasing ion fluences up to a particular value and beyond that value, it showing

suppression in PL-intensity along with peak broadening. The increase in PL intensity of visible emission band for the ion fluence of 3×10^{11} ions/cm 2 could be due to the generation of radiative recombination centers in the system. While suppression in PL-intensity above the ion fluence of 3×10^{11} ions/cm 2 could be attributed to the formation of non-radiative defects due to energy deposition via heavy ion irradiation. However, there is no observable change in peak shift is observed after ion irradiation.

On the other hand, for the case of films annealed at 700 °C (Set-C and Set-D) irradiated with Ni and Au ions the behavior of visible emission is found to be a bit different. In the case of these films, the PL intensity going to decrease with increasing ion fluences for both the ions as can be seen from Fig. 5(c) and (d). As can be seen from this figure that in the case of Au ions irradiated films (Set-D) the PL intensity is much lower than Ni ions irradiated films although the response is the same for both the ions. The high intensity in the case of Au ions irradiated films attributed to the creation of a high density of defects than Ni ions irradiated films. As the electronic energy loss is 2 times higher for Au ions into ZnO than Ni ions as already discussed in the experimental section. Further, there is an observable peak shifting of a maximum of visible emission band from green emission region (510 nm) to red emission region (around 630 nm) at low fluence. While at higher fluence the maximum of visible emission band again starts shifting to green emission region from the red emission region. For better clarity, the PL-spectra of Set-C and Set-D samples are zoomed for films irradiated at higher fluences and shown in Fig. 6(a) and (b), respectively. As can be seen that in the case of Au irradiated films (Set-D samples) the peak shifting from red to green emission takes place at moderate ion fluences in comparison to Ni-irradiated films (Set-C samples) in which the red to green emission take place at higher fluence. This could be attributed to the higher value of electronic energy loss in the case of Au ions which causes more density of defects even at lower or moderate fluence than Ni ion.

Moreover, with all these PL results we tried to understand what is the

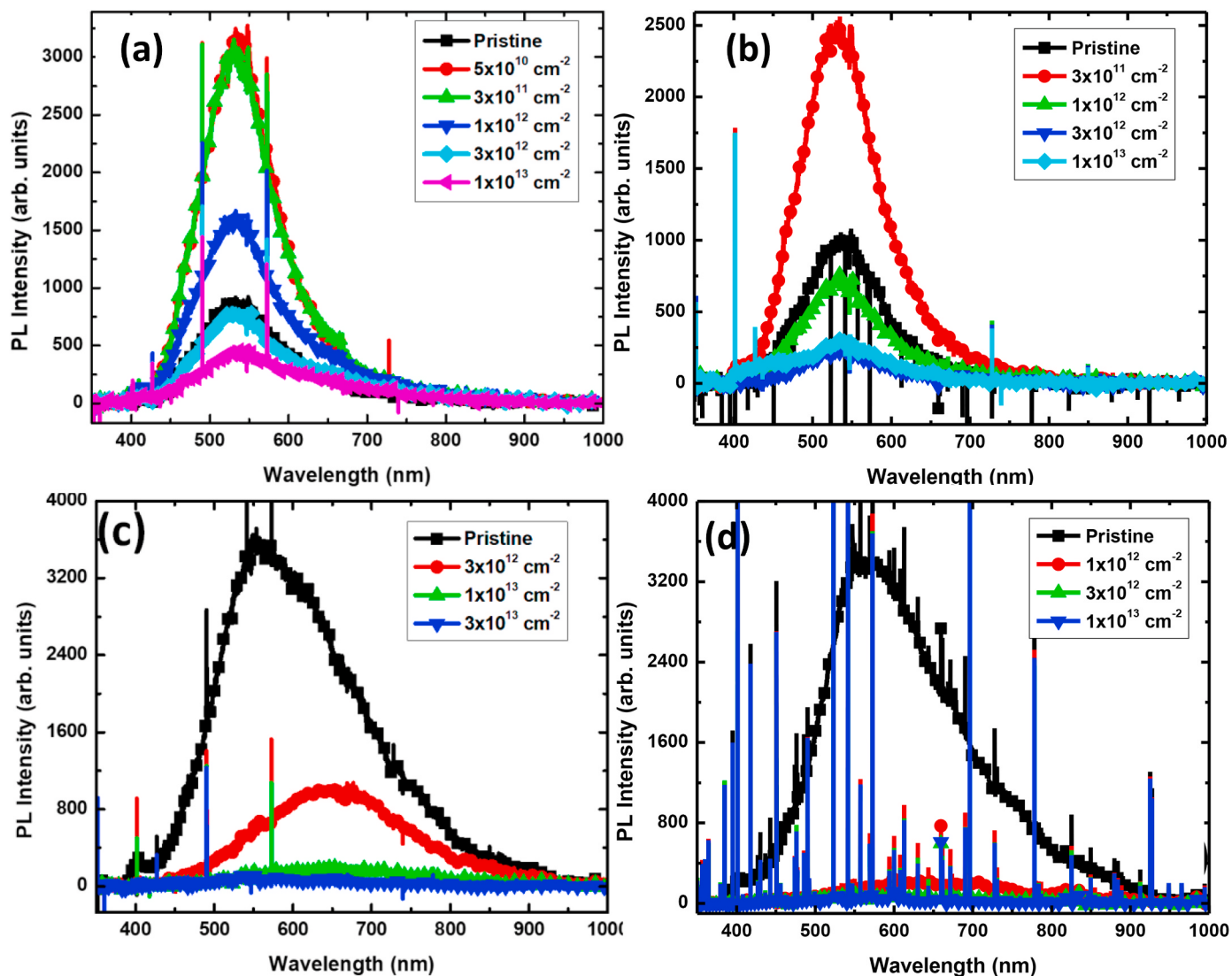


Fig.-5. PL spectra of; (a) 500 °C–Ar annealed films irradiated with 50 MeV–Ni ions (Set-A), (b) 500 °C–Ar annealed films irradiated with 120 MeV–Au ions (Set-B), (c) 700 °C–Ar annealed films irradiated with 50 MeV–Ni ions (Set-C), and (d) 700 °C–Ar annealed films irradiated with 120 MeV–Au ions (Set-D).

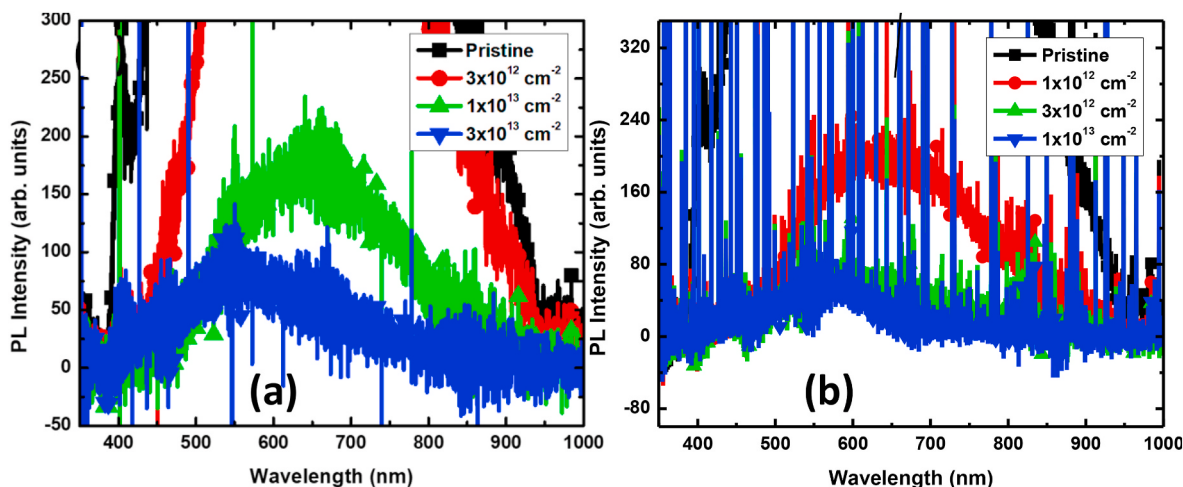


Fig.-6. Zoomed PL spectra of; (a) samples of Set-C and (b) samples of Set-D.

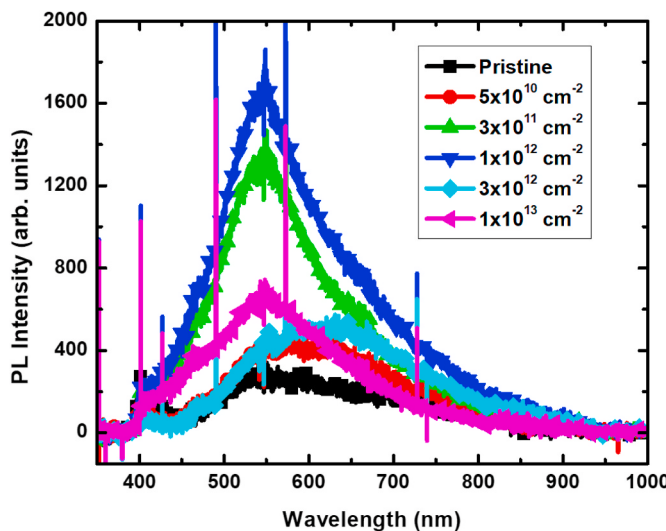


Fig.-7. PL spectra of 500 °C-oxygen annealed films irradiated with 50 MeV–Ni ions (Set-E).

possible origin of the green emission band in ZnO. As the origin of green emission in ZnO is contradictory in many reports so it is essential to understand it in detail for the further development of ZnO based light-emitting devices. In literature there are many assumptions regarding the origin of green emission like in some reports suggested copper (Cu^{2+}) impurity (Dingle, 1969; Huang et al., 2013) as the responsible defect for green emission while some reports believe that green emission originates from ZnO intrinsic defects such as V_{Zn} (Čížek et al., 2015; Rodnyi and Khodyuk, 2011), V_O (Gupta et al., 2019; Ye et al., 2005; Leiter et al., 2001), and transition from Zn_i to V_O^{43} . However, in the present case, the increase in green emission intensity with increasing annealing temperature and ion irradiation also indicates that the possible origin for green emission is oxygen vacancies which act as a deep donor in ZnO. Further to reaffirm it we also study PL-spectra of Ni-irradiated ZnO films annealed in an oxygen environment (Set-E samples) as shown in Fig.-7. As can be seen in this figure that in the case of pristine sample the intensity of green emission is lower than the pristine samples annealed in Ar-environment. While with the ion irradiation the intensity of Set-E samples increases up to the moderate ion fluence of 1×10^{12} ions/cm (Hüpkes et al., 2012), which vindicated oxygen vacancies as a possible origin of green emission in ZnO. As it is well known that in the case of ZnO irradiated with SHI the formation of oxygen vacancies takes place more easily than other defects (Singh et al., 2011b). Although, at the higher fluences the shifting of a maximum of visible emission from green emission peak to red emission peak is also observed in this case. This is happening because at higher fluences the formation of more complex defects takes place such as defect clusters and their pair (Gautam et al., 2015).

4. Conclusions

The effect of annealing temperature, annealing environment, and swift heavy ion irradiation on the luminescence properties of ZnO thin films are systematically studied. XRD pattern showed that all the films were polycrystalline. The average grain size was increased with annealing temperature, while it shows reduction upon ion irradiation with Au ions. Also, films irradiated with Au ions exhibit stress and strain along the c-axis in the film. The presence of stress and strain in the case of Au-irradiated film was attributed to the increase in surface roughness with increasing ion fluence which is supported by AFM study. Further, from the PL study the increase in visible emission with an increase in annealing temperature and ion irradiation at low fluences were reported. From the present, it is clear that the green emission is more

pronounced in the reduced annealing environment and its intensity could be enhanced by increasing annealing temperature as well as via ion irradiation at low ion fluences.

CRediT authorship contribution statement

R.G. Singh: Investigation, Data curation, Formal analysis, Writing – original draft. Himanshi Gupta: Resources, Validation. R.M. Mehra: Conceptualization, Visualization, Supervision. Fouran Singh: Conceptualization, Investigation, Visualization, Formal analysis, Writing – review & editing.

Declaration of competing interest

The authors declare that they have no known competing financial interests or personal relationships that could have appeared to influence the work reported in this paper.

Acknowledgments

The authors are grateful to Dr. D. K. Avasthi for the moral encouragements and Dr. A. Tripathi for the experimental support in AFM investigations. The authors are also thankful to the Pelletron group of IUAC for providing a stable beam during the irradiation experiment and IUAC for providing the beamtime through project: UFUP-37320..

Appendix A. Supplementary data

Supplementary data to this article can be found online at <https://doi.org/10.1016/j.radphyschem.2021.109400>.

References

- Ambrosio, R., Galindo, F., Morales-Morales, F., Moreno, M., Torres, A., Vásquez-A, M.A., Pérez García, S.A., Morales-Sánchez, A., 2019. Effect of the thermal annealing on the structural, morphological and photoluminescent properties of ZnO/Si multilayers. Opt. Mater. 96, 109339.
- Barbagiovanni, E.G., Strano, V., Franzò, G., Crupi, I., Mirabella, S., 2015. Photoluminescence transient study of surface defects in ZnO nanorods grown by chemical bath deposition. Appl. Phys. Lett. 106, 093108.
- Bhosle, V., Prater, J.T., Yang, F., Burk, D., Forrest, S.R., Narayan, J., 2007. Gallium-doped zinc oxide films as transparent electrodes for organic solar cell applications. J. Appl. Phys. 102, 023501.
- Cao, Y.-T., Cai, Y., Yao, C.-B., Bao, S.-B., Han, Y., 2019. The photoluminescence, field emission and femtosecond nonlinear absorption properties of Al-doped ZnO nanowires, nanobelts, and nanoplane-cone morphologies. RSC Adv. 9, 34547–34558.
- Čížek, J., Valenta, J., Hruška, P., Melikhova, O., Procházka, I., Novotný, M., Bulíř, J., 2015. Origin of green luminescence in hydrothermally grown ZnO single crystals. Appl. Phys. Lett. 106, 251902.
- Dingle, R., 1969. Luminescent transitions associated with divalent copper impurities and the green emission from semiconducting zinc oxide. Phys. Rev. Lett. 23, 579–581.
- Fan, X.M., Lian, J.S., Guo, Z.X., Lu, H.J., 2005. Microstructure and photoluminescence properties of ZnO thin films grown by PLD on Si (1 1 1) substrates. Appl. Surf. Sci. 239, 176–181.
- Gautam, S.K., Singh, R.G., Siva Kumar, V.V., Singh, F., 2015. Giant enhancement of the n-type conductivity in single phase p-type ZnO:N thin films by intentionally created defect clusters and pairs. Solid State Commun. 218, 20–24.
- Gruzintsev, A.N., Yakimov, E.E., 2005. Annealing effect on the luminescent properties and native defects of ZnO. Inorg. Mater. 41, 725–729.
- Gupta, H., Singh, J., Dutt, R.N., Ojha, S., Kar, S., Kumar, R., Reddy, V.R., Singh, F., 2019. Defect-induced photoluminescence from gallium-doped zinc oxide thin films: influence of doping and energetic ion irradiation. Phys. Chem. Chem. Phys. 21, 15019–15029.
- Gupta, H., Joshi, K., Gautam, S.K., Singh, R.G., Singh, F., 2020. Raman scattering from irradiated nanocrystalline zinc oxide thin films: perspective view on effects of energy loss, ion fluence, and ion flux. Vacuum 181, 109598.
- Hornig, R.H., Ou, S.L., Huang, C.Y., Ravadgar, P., Wu, C.I., 2016. Effects of Ga concentration and rapid thermal annealing on the structural, optoelectronic and photoluminescence properties of Ga-doped ZnO thin films. Thin Solid Films 605, 30–36.
- Huang, X.H., Zhang, C., Tay, C.B., Venkatesan, T., Chua, S.J., 2013. Green luminescence from Cu-doped ZnO nanorods: role of Zn vacancies and negative thermal quenching. Appl. Phys. Lett. 102, 111106.
- Hüpkes, J., Owen, J.I., Pust, S.E., Bunte, E., 2012. Chemical etching of zinc oxide for thin-film silicon solar cells. ChemPhysChem 13, 66–73.

- Janotti, A., Van de Walle, C.G., 2007. Native point defects in ZnO. *Phys. Rev. B* 76, 165202.
- Kabir, A., Bouanane, I., Boulainine, D., Zerkout, S., Schmerber, G., Boudjema, B., 2018. Photoluminescence study of deep level defects in ZnO thin films. *Siliconindia* 1–6.
- Kang, H.S., Kang, J.S., Kim, J.W., Lee, S.Y., 2004. Annealing effect on the property of ultraviolet and green emissions of ZnO thin films. *J. Appl. Phys.* 95, 1246–1250.
- Khranovskyy, V., Sendova, M., Hosterman, B., McGinnis, N., Shtepliuk, I., Yakimova, R., 2017. Temperature dependent study of basal plane stacking faults in Ag:ZnO nanorods by Raman and photoluminescence spectroscopy. *Mater. Sci. Semicond. Process.* 69, 62–67.
- Kim, J.-H., Shin, T.-H., Yang, K.-J., Jeong, J., Choi, B., 2012. Abstraction of blue photoluminescence in Al-doped ZnO nanoparticles prepared by electron beam deposition. *APEX* 5, 012603.
- Kumar, V., Singh, F., Ntwaeborwa, O.M., Swart, H.C., 2013a. Effect of Br+6 ions on the structural, morphological and luminescent properties of ZnO/Si thin films. *Appl. Surf. Sci.* 279, 472–478.
- Kumar, V., Singh, R.G., Purohit, L.P., Singh, F., 2013b. Effect of swift heavy ion on structural and optical properties of undoped and doped nanocrystalline zinc oxide films. *Adv. Mater. Lett.* 4, 423–427.
- Leiter, F.H., Alves, H.R., Hofstaetter, A., Hofmann, D.M., Meyer, B.K., 2001. The oxygen vacancy as the origin of a green emission in undoped ZnO. *Phys. Status Solidi Basic Res.* 226, 5–6.
- Look, D.C., Farlow, G.C., Reunchan, P., Limpijumnong, S., Zhang, S.B., Nordlund, K., 2005. Evidence for Native-Defect Donors in n -Type ZnO. *Phys. Rev. Lett.* 95, 225502.
- Lyons, J.L., Varley, J.B., Steiauf, D., Janotti, A., Van de Walle, C.G., 2017. First-principles characterization of native-defect-related optical transitions in ZnO. *J. Appl. Phys.* 122, 035704.
- Musavi, E., Khanlary, M., Khakpour, Z., 2019. Red-orange photoluminescence emission of sol-gel dip-coated prepared ZnO and ZnO:Al nano-crystalline films. *J. Lumin.* 216, 116696.
- Naik, E.I., Naik, H.S.B., Viswanath, R., Gowda, I.K.S., Prabhakara, M.C., 2020. Bright red luminescence emission of macroporous honeycomb-like Eu³⁺ ion-doped ZnO nanoparticles developed by gel-combustion technique. *SN Appl. Sci.* 2, 863.
- Oba, F., Choi, M., Togo, A., Tanaka, I., 2011. Point defects in ZnO: an approach from first principles. *Sci. Technol. Adv. Mater.* 12, 034302.
- Özgür, Ü., Alivov, Y.I., Liu, C., Teke, A., Reschchikov, M.A., Doğan, S., Avrutin, V., Cho, S.-J., Morkoç, H., 2005a. A comprehensive review of ZnO materials and devices. *J. Appl. Phys.* 98, 041301.
- Özgür, Ü., Alivov, Y.I., Liu, C., Teke, A., Reschchikov, M.A., Doğan, S., Avrutin, V., Cho, S.-J., Morkoç, H., 2005b. A comprehensive review of ZnO materials and devices. *J. Appl. Phys.* 98, 041301.
- Rodnyi, P.A., Khodyuk, I.V., 2011. Optical and luminescence properties of zinc oxide (Review). *Optic Spectrosc.* 111, 776–785.
- Ryu, Y., Lee, T., Lubguban, J.A., White, H.W., Kim, B., Park, Y., Youn, C.-J., 2006. Next generation of oxide photonic devices: ZnO-based ultraviolet light emitting diodes. *Appl. Phys. Lett.* 88, 241108.
- Sharma, S., Vyas, R., Shrivastava, S., Vijay, Y.K., 2011. Effect of swift heavy ion irradiation on photoluminescence properties of ZnO/PMMA nanocomposite films. *Phys. B Condens. Matter* 406, 3230–3233.
- Shishiyaru, S.T., Shishiyaru, T.S., Lapan, O.I., 2005. Sensing characteristics of tin-doped ZnO thin films as NO₂ gas sensor. *Sensor. Actuator. B Chem.* 107, 379–386.
- Singh, R.G., Singh, F., Sulania, I., Kanjilal, D., Sehrawat, K., Agarwal, V., Mehra, R.M., 2009. Electronic excitations induced modifications of structural and optical properties of ZnO-porous silicon nanocomposites. *Nucl. Instrum. Methods Phys. Res. Sect. B Beam Interact. Mater. Atoms* 267, 2399–2402.
- Singh, R.G., Singh, F., Kumar, V., Mehra, R.M., 2011a. Growth kinetics of ZnO nanocrystallites: structural, optical and photoluminescence properties tuned by thermal annealing. *Curr. Appl. Phys.* 11, 624–630.
- Singh, F., Singh, R.G., Kumar, V., Khan, S.A., Pivin, J.C., 2011b. Softening of phonons by lattice defects and structural strain in heavy ion irradiated nanocrystalline zinc oxide films. *J. Appl. Phys.* 110, 083520.
- Soni, A., Mulchandani, K., Mavani, K.R., 2020. UV activated visible-blind Ga:ZnO photodetectors using the GLAD technique: a comparative study in different gas atmospheres and temperatures. *J. Mater. Chem. C* 8, 7837–7846.
- Thandavan, T.M.K., Gani, S.M.A., Wong, C.S., Nor, R.M., 2015. Evaluation of Williamson–Hall strain and stress distribution in ZnO nanowires prepared using aliphatic alcohol. *J. Nondestr. Eval.* 34, 14.
- Thongpool, V., Phunpuueok, A., Jaiyen, S., 2019. Photoluminescence of ZnO nanorods prepared by hydrothermal method. *J. Phys. Conf. Ser.* 1380, 012052.
- Vanhusden, K., Seager, C.H., Warren, W.L., Tallant, D.R., Voigt, J.A., 1996. Correlation between photoluminescence and oxygen vacancies in ZnO phosphors. *Appl. Phys. Lett.* 68, 403–405.
- Vettumperumal, R., Kalyanaraman, S., Thangavel, R., 2014. Photoconductive UV detectors based heterostructures of Cd and Mg doped ZnO sol gel thin films. *Mater. Chem. Phys.* 145, 237–242.
- Willander, M., Nur, O., Zhao, Q.X., Yang, L.L., Lorenz, M., Cao, B.Q., Ziga Pérez, J., Czekalla, C., Zimmermann, G., Grundmann, M., Bakin, A., Behrends, A., Al-Suleiman, M., El-Shaer, A., Che Mofor, A., Postels, B., Waag, A., Boukos, N., Travlos, A., Kwack, H.S., Guinard, J., Le Si Dang, D., 2009. Zinc oxide nanorod based photonic devices: recent progress in growth, lightemitting diodes and lasers. *Nanotechnology* 20, 332001.
- Xu, W.Z., Ye, Z.Z., Zeng, Y.J., Zhu, L.P., Zhao, B.H., Jiang, L., Lu, J.G., He, H.P., Zhang, S. B., 2006. ZnO light-emitting diode grown by plasma-assisted metal organic chemical vapor deposition. *Appl. Phys. Lett.* 88, 173506.
- Ye, J.D., Gu, S.L., Qin, F., Zhu, S.M., Liu, S.M., Zhou, X., Liu, W., Hu, L.Q., Zhang, R., Shi, Y., Zheng, Y.D., 2005. Correlation between green luminescence and morphology evolution of ZnO films. *Appl. Phys. Mater. Sci. Process* 81, 759–762.
- Zhu, L., Zeng, W., 2017. Room-temperature gas sensing of ZnO-based gas sensor: a review. *Sensors Actuators A Phys* 267, 242–261.